photonics

IMPACT FACTOR 2.1

CITESCORE 2.6

Article

Direct Acceleration of an Electron Beam with a Radially Polarized Long-Wave Infrared Laser

William H. Li, Igor V. Pogorelsky and Mark A. Palmer

Special Issue
High Power Lasers: Technology and Applications

Edited by
Dr. Changqing Cao

MDPI

https://doi.org/10.3390/photonics11111066

photonics

MDPI

Article

Direct Acceleration of an Electron Beam with a Radially Polarized Long-Wave Infrared Laser

William H. Li *, Igor V. Pogorelsky and Mark A. Palmer

Accelerator Test Facility, Brookhaven National Laboratory, Upton, NY 11973, USA; igor@bnl.gov (I.V.P.); mpalmer@bnl.gov (M.A.P.)

* Correspondence: wli4@bnl.gov

Abstract: Direct laser acceleration with radially polarized lasers is an intriguing variant of laser-based particle acceleration that has the potential of offering GeV/cm-level energy while avoiding the instabilities and complex beam dynamics associated with plasma wakefield accelerators. A major limiting factor is the difficulty of generating high-power radially polarized beams. In this paper, we propose the use of CO_2-based long-wave infrared (LWIR) lasers as a driver for direct laser acceleration, as the polarization insensitivity of the gain medium allows a radially polarized beam to be amplified. Additionally, the larger waist sizes, Rayleigh lengths, and pulse lengths associated with the long wavelength could improve the injection efficiency of the electron beam. By comparing acceleration simulations using a near-infrared laser and an LWIR laser, we show that the injection efficiency is indeed improved by up to an order of magnitude with the longer wavelength. Furthermore, we show that even sub-TW peak powers with an LWIR laser can provide MeV-level energy gains. Thus, radially polarized LWIR lasers show significant promise as a driver of a direct laser-driven demonstration accelerator.

Keywords: long-wave infrared; radial polarization; direct laser acceleration

Citation: Li, W.H.; Pogorelsky, I.V.; Palmer, M.A. Direct Acceleration of an Electron Beam with a Radially Polarized Long-Wave Infrared Laser. *Photonics* **2024**, *11*, 1066. https://doi.org/10.3390/photonics11111066

Received: 18 October 2024
Revised: 8 November 2024
Accepted: 12 November 2024
Published: 14 November 2024

1. Introduction

Vector laser beams, laser beams with spatially dependent polarization, have many interesting attributes that set them apart from their conventional linearly or circularly polarized counterparts. In particular, cylindrically symmetric vector beams, such as radially and azimuthally polarized beams, have opened new regimes in applications such as particle trapping [1–3] and laser machining [4–7], due to their unique spatial profiles, tighter focuses [8,9], and strong longitudinal field components [10,11].

One intriguing application of radially polarized beams is their use in particle acceleration [10,12–15]. Currently, the primary area of research in particle acceleration with high-intensity lasers is laser plasma wakefield acceleration [16], where a high-intensity laser interacting with a plasma ponderomotively drives electrons away from its central axis, generating GV/cm-level fields in the region of depleted electrons [17,18]. A major challenge for this scheme is the instabilities introduced by the presence of the plasma and the associated complex beam dynamics [19]. Laser acceleration in vacuum bypasses this issue, while still potentially offering up to GeV-level energy gain over a few mm [10].

The removal of the plasma presents its own challenge, summarized in the Lawson–Woodward theorem. The Lawson–Woodward theorem essentially states that under certain assumptions, namely, an infinite vacuum interaction region far from walls or boundaries with an ultrarelativistic electron beam and excluding nonlinear effects, no net energy gain can be imparted to an electron beam by an electromagnetic wave [20,21]. Thus, efforts in direct laser acceleration must break one or more of these assumptions to produce a net energy gain.

A simple way to violate one of the Lawson–Woodward assumptions is to accelerate electrons from rest, which violates the assumption that the electron beam is ultrarelativistic

at all times. This has been experimentally demonstrated, with stationary electrons accelerated to MeV-level energies with an intense linearly polarized laser [22]. This acceleration mechanism consists of three parts: a ponderomotive pushing of the electrons away from the axis of the laser, bending of the trajectories by the magnetic field of the laser, and a final push by the longitudinal component of the laser field [23,24]. Due to the inherent transverse motion involved in this process, the electron beam typically exhibits a large divergence after acceleration. The use of radially polarized beams has thus been proposed in order to take advantage of the stronger longitudinal field and transverse confinement by the radial fields [10,21,24–26]. A proof-of-principle demonstration of acceleration with radially polarized beams was carried out and, indeed, showed the expected transverse confinement [12]. Recent work has demonstrated the use of a radially polarized beam to ionize electrons from a gas and accelerate them to up to 1.43 MeV [27].

In 2010, Wong and Kärtner developed an analytic model for the acceleration of an electron by the longitudinal electric field of a radially polarized laser under the paraxial approximation [15]. In this model, the laser is fully characterized with six parameters: the wavelength λ, the pulse length τ, the waist radius w_0, the initial position z_i, the carrier-envelope phase ψ_0, and the peak power P. Notably, this model predicts that for a given peak power, changing the wavelength has no effect on energy gain as long as the wavelength-normalized focusing (w_0/λ) and number of cycles in the pulse, ωt, remain constant. Furthermore, while previous studies had focused on initially stationary electrons, this study found that the energy gain could be significantly enhanced by using pre-accelerated electrons.

While it may seem that the further acceleration of ultrarelativistic particles would run afoul of the Lawson–Woodward theorem, Wong and Kärtner found that the electrons pass through a decelerating phase where their velocity drops to nonrelativistic levels before their final accelerating phase to achieve net energy gain; thus, the assumption of an ultrarelativistic electron beam remains violated. Although, in principle, this could be used for linearly polarized beams as well, the energy gain is smaller and divergence much larger than for an equivalent radially polarized beam (see Appendix B). Thus, to maintain high-quality electron beams throughout the acceleration process, radially polarized lasers are necessary.

Currently, progress in this acceleration method has been limited by the difficulty of generating high-power radially polarized beams. The highest peak powers reported have typically been less than 100 GW [28,29], well below the TW-level peak powers that were predicted to allow for MeV-level energy gain in the paraxial regime [15], and far below the PW-level peak powers achievable with conventional linearly polarized lasers that would be necessary for GeV-level energy gain. Recently, this barrier was broken with the production of 27 TW using a segmented waveplate, resulting in 2 MeV energy electrons ejected from a plasma mirror by a radially polarized beam [30]. Due to the polarization sensitivity of most common laser gain media, the conversion from linear polarization to radial polarization must take place after amplification, as, otherwise, a specific linear polarization would be preferentially amplified, washing out the spatial dependence [29]. Thus, the peak power will be limited by the damage thresholds of the polarization optics.

A potential path forward lies in using a long-wave infrared (LWIR) CO_2 laser instead of a typical near-infrared (NIR) titanium–sapphire (Ti:Sa) laser. As a gas, CO_2 is polarization insensitive and, thus, the conversion to radial polarization can be carried out at low power before subsequent amplification in the CO_2 [31]. Conversion of a low-power LWIR laser to radial polarization has been demonstrated with 70% efficiency [32]. While the gratings used in chirped pulse amplification (CPA) schemes cannot be used for radially polarized beams due to their polarization sensitivity [29], CO_2, by virtue of being a gas, can sustain much higher peak powers than conventional solid gain media, with 15 TW peak powers (linearly polarized) having been demonstrated in a direct amplification mode [33]. Peak powers in this regime are typically limited by pulse length, typically a few picoseconds, not by pulse energy, which is regularly at the multi-joule level [33,34]. LWIR technology is

rapidly developing and could potentially scale to peak powers beyond the limits imposed by damage thresholds for NIR radially polarized beams.

Furthermore, changing from an NIR to an LWIR laser, although requiring substantially more pulse energy to generate the same peak power (holding the number of cycles in the pulse fixed), could result in better acceleration efficiency due to the larger size of the focus and longer Rayleigh range accepting a larger proportion of the electron beam. In this paper, we compare the acceleration properties of a Ti:Sa laser and a CO_2 laser and simulate a potential proof-of-concept demonstration that can be carried out at the Accelerator Test Facility (ATF) in the near future.

2. Methods

For these simulations, we employ the ASTRA code [35], a particle tracking code with an efficient algorithm for space charge calculations as well as a built-in paraxial radially polarized laser module. Benchmarks of the radially polarized laser module can be found in Appendix A.

While using a laser in the nonparaxial regime can result in higher energy gain [24,27,36], our intended purpose is to compare a Ti:Sa and CO_2 laser for a direct laser accelerator that a pre-accelerated beam is coupled into. This setup is useful for high bunch charges, such as for free electron lasers or colliders, due to the ability to generate a millimeter-scale beam in an rf gun, mitigating space charge effects, before focusing into the direct laser accelerator. Additionally, multi-stage acceleration may be necessary for collider energies and would inherently require coupling the electron beam into the direct laser accelerator. Since having a larger waist will benefit the coupling efficiency, as we will see later in this paper, we look only at laser parameters where the paraxial approximation remains valid. For low charge, MeV-scale applications such as diffraction, accelerating electrons from rest using a nonparaxial laser may be a superior alternative.

The simulations can be split into two sections. First, we compare the acceleration efficiency of a Ti:Sa ($\lambda = 800$ nm) and a CO_2 ($\lambda = 9.2$ μm) laser for a beam with realistic spatial extent. For the comparison between Ti:Sa and CO_2, we set the electron beam energy to 7 MeV, a typical output energy of a modern rf electron gun [37,38], as we are focusing on the use of a direct laser accelerator to replace the rf linac without replacing the electron source. We use 2×10^4 macroparticles in a beer can distribution with a length of 10 μm and vary the laser peak power and the electron beam diameter. To simplify the comparison, the electrons have zero initial transverse momentum and zero energy spread, and space charge effects are neglected.

Previous work has found that, in general in the paraxial regime, the maximum acceleration increases with a tighter focus [10,15], while increasing the pulse length actually increases the energy gain until an optimal pulse length is reached, after which it again decreases. We will use parameters found to be roughly optimal in ref. [15] for a Ti:Sa laser, namely $w_0 = 2$ μm and $\tau = 7.5$ fs. We will compare this to a CO_2 laser with the same w_0/λ and $\omega\tau$, corresponding to physical values of $w_0 = 23$ μm and $\tau = 86$ fs, with the same peak power. We will also examine a Ti:Sa with $w_0 = 23$ μm and $\tau = 86$ fs to determine if simply increasing the size of the laser can improve the electron beam acceptance or if the scaling of maximum acceleration renders this ineffective. The simulation start position is set well before the laser intensity is high enough to impact the electron energy and the end position is set after the electron beam has reached an equilibrium energy. The offset between the initial positions of the laser and electron beam and the carrier-envelope phase are set by optimizing the single-particle energy gain. The simulation timestep used is 0.01 fs for the Ti:Sa simulation and 0.115 fs for the CO_2 simulation, thus keeping the total number of timesteps in each case constant.

The second part consists of simulating a direct laser acceleration experiment that could be performed at the ATF in the near future. The ATF contains both a 70 MeV electron beam linac and a terawatt-class CO_2 laser [34,39], with the capability of delivering both beams to the same interaction point. On the electron beam side, we examine two electron

beam energies: 7 MeV at the exit of the gun and 20 MeV, which is approximately the minimum energy deliverable to the interaction point without reconfiguring the beamline. We use a bunch charge of 100 pC with 2×10^5 macroparticles in a beer can distribution with a diameter of 10 μm and a length of 1 ps, comparable to beam sizes that have been achieved in the past [40]. Space charge effects are included. The electrons have zero initial transverse momentum, and the relative energy spread is set to 2×10^{-3}. Due to the low laser intensities involved in this set of simulations, a timestep of 11.5 fs is sufficient for the simulation accuracy to converge.

Currently, the ATF CO_2 laser is able to produce roughly 5 TW peak powers. Accounting for the losses in the conversion to radially polarized light and the reduced amplification due to the inability to use CPA, we expect that 1 TW peak power should be achievable. We will simulate this experiment with both a 1 TW peak power and a more conservative 0.5 TW and determine whether a substantial energy modulation will be achievable. In both cases, we will use a FWHM pulse length of 2 ps, corresponding to the typical running conditions at the ATF.

3. Results

3.1. Comparison of Ti:Sa and CO_2

To quantify the comparison between direct laser acceleration using Ti:Sa and CO_2, we define particles to be "high energy" if they have gained at least 10% of the theoretical gain limit, given by the equation [13,15]

$$\Delta E_{lim}[\text{GeV}] \approxeq \sqrt{P[\text{PW}]}. \tag{1}$$

Note that this represents the energy gain achieved by a particle that remains perfectly at the peak of the pulse and stays in phase with the laser for all time. Realistically, the maximum energy gain would be limited by slippage and typically sits between 0.2 and 0.6 times this value.

The overall acceleration efficiency can be defined either with the fraction of particles that achieve high energy or by the average energy gain of the beam. For completeness, we will consider both. The results are shown in Figure 1. Each column corresponds to a different electron beam diameter, indicated by the upper label. We see that the CO_2 laser is capable of achieving at least 10% high-energy particles in every case, often even in the 60–70% range for a small electron beam. By contrast, the Ti:Sa is unable to achieve more than around 10% high-energy particles in any case and is usually in the single-digit or sub-percent levels. In nearly every set of parameters, the CO_2 laser generates around an order of magnitude more high-energy particles than the Ti:Sa laser by virtue of the larger acceptance.

A similar situation plays out if we examine the average energy gain imparted to the beam. The CO_2 laser typically produces 3–4 times higher energy gain across electron beam diameters and laser powers. The difference is particularly noticeable at large electron beam diameters. While it is expected that the larger size of the CO_2 laser would allow the electron beam to couple in more efficiently, the magnitude of the effect is nonetheless remarkable.

An interesting feature of these plots is that the acceleration efficiency as measured by the high-energy fraction appears to depend only weakly on the electron beam diameter at high peak powers, while there is a substantial change at low peak powers. This effect is consistent for both wavelengths, with the drop in efficiency being more pronounced for the Ti:Sa, consistent with its smaller waist size. Thus, the problem of injecting the electron beam into the laser is actually more difficult at low peak powers. However, at any power, the ease of injection offered by the CO_2 laser still yields substantial efficiency enhancement.

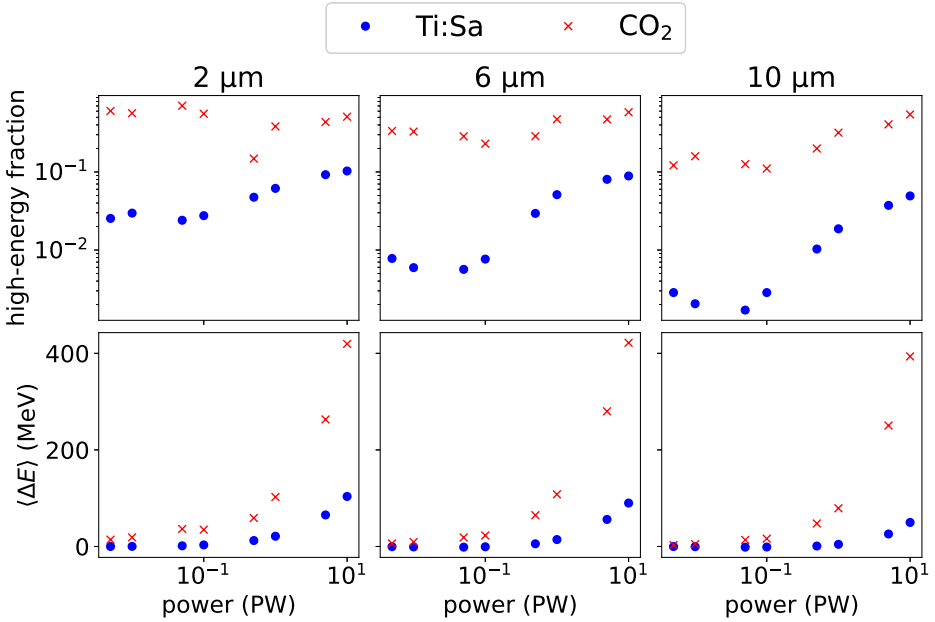

Figure 1. Comparison of Ti:Sa and CO_2 direct laser acceleration efficiency. Column titles refer to the electron beam diameter. The term "high-energy fraction" refers to the fraction of the beam that has gained at least 10% of the theoretical gain limit and is used here as a measure of acceleration efficiency. The high-energy fraction of the CO_2 laser is at least 2 times higher than for the Ti:Sa laser at all simulated powers and electron beam diameters, and is almost always 5–10 times higher. The average energy gain is correspondingly higher for the CO_2 laser as well.

To provide some more insight, we turn now to examining the distribution of electron energies for a few selected cases. These distributions are shown in Figure 2. Here, we see that the majority of electrons see almost no acceleration from the Ti:Sa laser, while almost all electrons see at least some amount of acceleration from the CO_2 laser. The non-accelerated portion of the beam does not even form a plurality of the beam accelerated by the CO_2 laser, with only one exception.

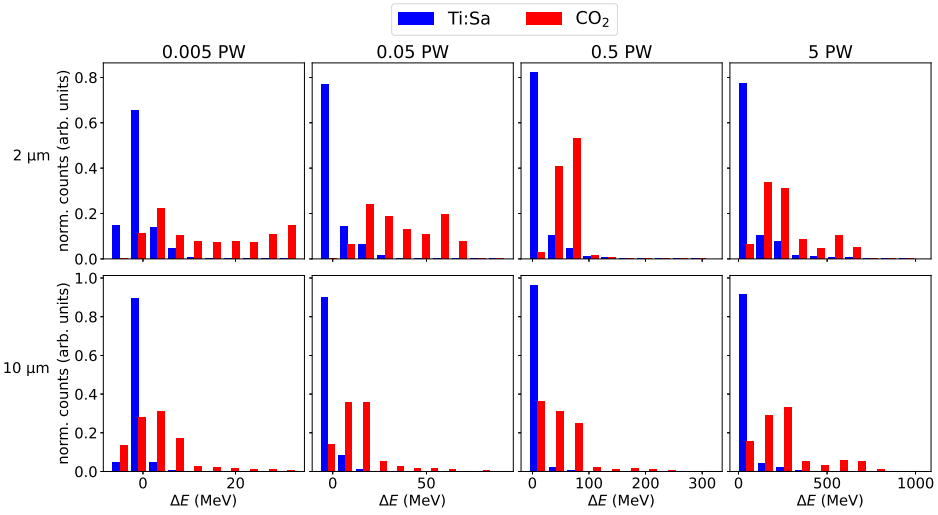

Figure 2. Energy distributions for some selected peak powers and electron beam diameters. Plots in the same row have the same electron beam diameter and plots in the same column have the same laser peak power. It is clear that, for the Ti:Sa laser, a large portion of the electron beam essentially does not participate in the acceleration interaction, while for the CO_2 laser, the majority of the beam is accelerated to some degree.

A striking feature is the much broader energy spectrum of the electrons at a 2 μm electron beam diameter compared to the 10 μm electron beam diameter for both wavelengths, coupled with the peak shifting to significantly higher energies. This is due to the 10 μm length of the electron beam causing it to sample a large portion of the longitudinal field distribution. Compression of the electron beam past this point is difficult, so it is likely that an energy selector, i.e., a slit in a bending section, after the acceleration stage would be necessary. The broadening is weaker at high peak powers, so the energy filtering may only be necessary for low power, depending on the application.

We now look at the scenario of increasing the size of the Ti:Sa focus and pulse length to improve the electron beam acceptance. A plot of the energy distribution of a 2 μm initial diameter electron beam interacting with a 10 PW Ti:Sa with $w_0 = 23$ μm and $\tau = 7.5$ fs is shown in Figure 3. We see that, while more of the electron beam fits into the laser focus, the strength of the acceleration falls too quickly with the increasing waist size and pulse length, resulting in negligible maximum energy gain: only on the order of 10 s of eV, even at this extreme power. This is consistent with the argument made in refs. [13,15] that a_0, the normalized vector potential, of the longitudinal E field at the focus must be at least 1 for acceleration to occur. The drastic drop in intensity from the 11.5 times increase in waist size causes the laser to no longer provide sufficient force to accelerate the electrons. In fact, while the transverse a_0 scales as $\sqrt{I\lambda^2}$, the longitudinal a_0 is given by $a_{0,z} \sim 0.742 a_{0,r}(\lambda_0/w_0)$, with an additional factor of $1/w_0$ [13]. Calculating $a_{0,z}$ with this formula gives us a value of 0.37, well below the necessary threshold value of 1. Due to the quadratic scaling of $a_{0,z}$ with wavelength, long wavelengths are necessary to take full advantage of the improved electron beam acceptance of a larger laser spot.

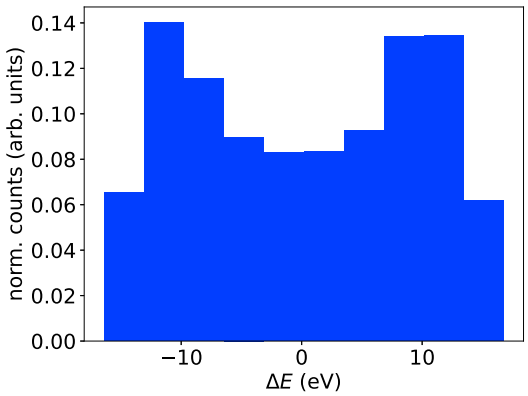

Figure 3. Energy distribution of a 2 μm initial diameter electron beam after interacting with a 10 PW Ti:Sa with $w_0 = 23$ μm and $\tau = 86$ fs. The electrons experience essentially no acceleration (note that the units on the x-axis are electron volts, not megaelectron volts).

3.2. Simulation of Potential Experiment

We look now at some proof-of-principle experiments that could be carried out with LWIR peak powers below even 1 TW. The acceleration performance can be quantified with the average energy gain $\langle \Delta E \rangle$ and the relative energy spread $\sigma_E / \langle E \rangle$. Along with these numbers, it is also useful to consider the transverse beam quality, encapsulated in the normalized rms emittance [41], defined as

$$\varepsilon_{n,x} = \frac{1}{mc} \sqrt{\langle x^2 \rangle \langle p_x^2 \rangle - \langle x p_x \rangle^2}, \tag{2}$$

where m is the rest mass of the electron and c is the speed of light. Since this quantity only provides information along one transverse axis, it is also useful to define a 6D brightness to incorporate both transverse and longitudinal beam quality [42,43].

$$B_{6D} = \frac{I}{\varepsilon_{n,x}\varepsilon_{n,y}0.1\%\frac{\sigma_E}{\langle E\rangle}}, \tag{3}$$

where I is the beam peak current and $\varepsilon_{n,x}$ and $\varepsilon_{n,y}$ are the normalized rms emittances in the x and y axes, respectively. Since particles in the beam are expected to have substantially different properties depending on the amount of energy gain received, we will plot these four figures of merit as a function of beam fraction, sorted by energy. Thus, for example, 10% on the x-axis of the plot indicates the 10% of particles with the highest energy. Practically, this kind of cut can be achieved using an energy selector, leading to a tradeoff between charge and beam quality.

The results of accelerating a beam with an initial energy of 7 MeV, corresponding to the exit of an rf gun, can be seen in Figure 4. At 0.5 TW, the majority of electrons have near-zero or negative energy gain, while at 1 TW, most electrons receive some positive energy gain. This is manifested in the roughly factor of 2 higher energy gain. However, the 1 TW laser causes more degradation in beam quality, as can be seen with the roughly 2 times larger energy spread, 2–5 times higher emittance, and roughly 100 times lower brightness. Both laser powers exhibit non-zero peak divergences, which can be attributed to space charge forces in the center of the beam. These space charge forces are greatly enhanced by the necessity of tightly focusing the electron beam to inject into the laser field at low peak powers. As seen in the previous section, high peak powers do not require the electron beam to be as small, and, thus, would not suffer as much from space charge-induced emittance degradation.

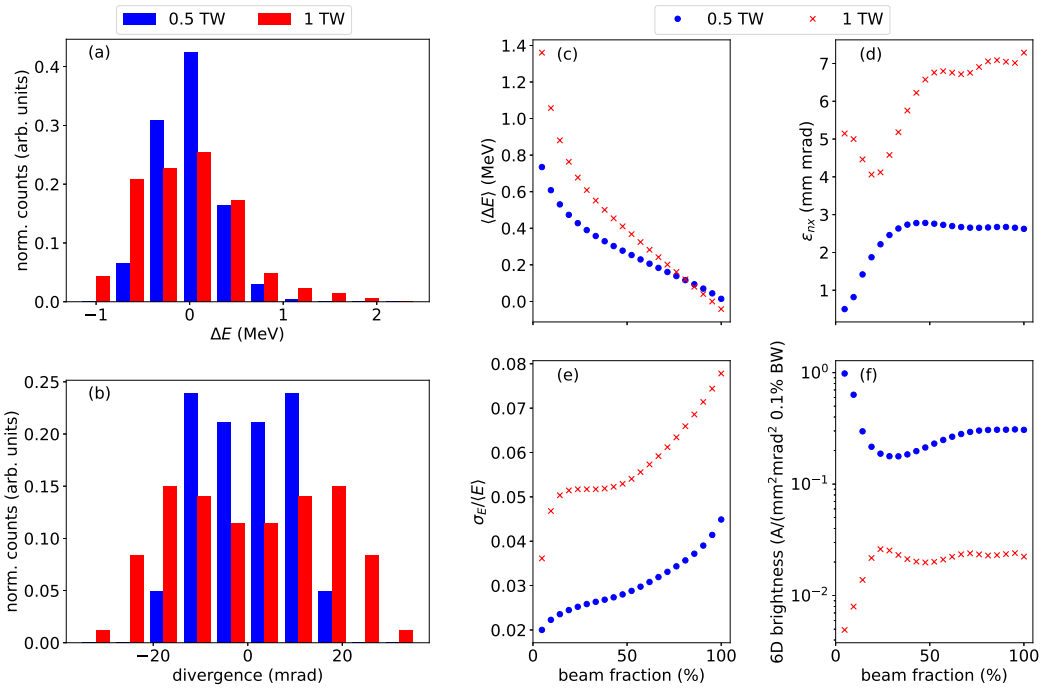

Figure 4. Final beam parameters of an accelerated electron beam with an initial energy of 7 MeV. (**a**) Electron energy distribution. (**b**) Electron beam divergence. (**c**–**f**) Electron beam parameters as a function of beam fraction (defined in the text). The peak energy gain is around a MeV for both laser powers used. The 0.5 TW laser, while providing around half the energy gain, allows for better beam quality.

The performance improves significantly when moving to 20 MeV, seen in Figure 5. Much of this improvement comes from the strong suppression of space charge effects at the higher electron beam energy. For both laser powers, the divergence is narrowed considerably and the distribution peaks along the axis. The reduction in divergence is

accompanied by a commensurate drop in emittance, around a factor of 30 for both laser powers, and a brightness enhancement of nearly three orders of magnitude.

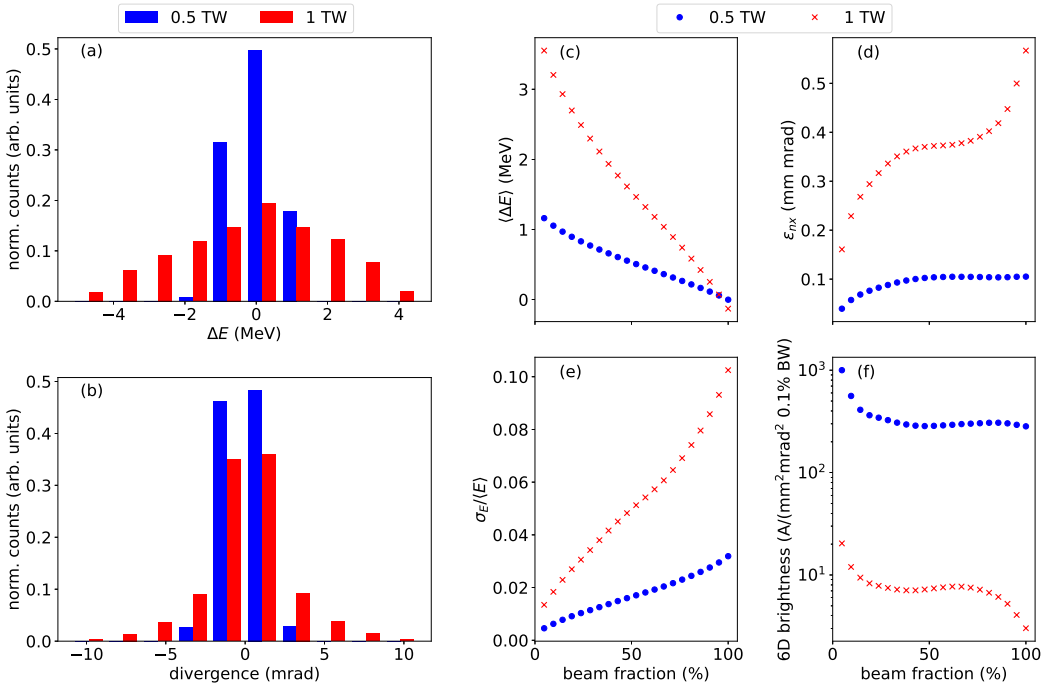

Figure 5. Final beam parameters of an accelerated electron beam with an initial energy of 20 MeV. (**a**) Electron energy distribution. (**b**) Electron beam divergence. (**c**–**f**) Electron beam parameters as a function of beam fraction (defined in the text). Compared to Figure 4, we see substantially improved acceleration and beam quality, and the 1 TW laser provides around 3 times the peak energy gain as the 0.5 TW laser.

As with the 7 MeV case, the 0.5 TW laser exhibits superior beam quality to the 1 TW laser. However, at 20 MeV, the 1 TW laser has a larger advantage in energy gain. While at 7 MeV, the peak energy gain for the 1 TW laser was a little less than two times larger than for the 0.5 TW laser, at 20 MeV, the 1 TW laser has over three times the energy gain. This is likely related to the hypothesis presented in ref. [15], stating that electrons with an initial energy substantially higher than the energy gain limit receive negligible energy gain due to the laser having insufficient power to decelerate the electrons to nonrelativistic velocities, a necessary step to achieve non-negligible energy gain. Since the theoretical gain limit for a 0.5 TW laser is roughly 22 MeV, the 20 MeV beam is nearing the limit beyond which the laser is no longer able to accelerate the electrons. Hence, the 1 TW laser, with a gain limit of around 31 MeV, now possesses an advantage in energy gain.

It is important to note that the emittances shown here, and correspondingly the brightnesses, represent the idealized limit of the direct laser accelerator performance. Realistically, the incoming electron beam will have some non-zero emittance that will affect the final beam quality. However, the emittances obtained here show that the direct laser accelerator will not degrade the beam quality noticeably for typical 1 mm mrad emittance beams.

4. Discussion

We turn now to some practical considerations regarding the use of an LWIR driver for direct laser acceleration, beginning with the generation of a terawatt-class radially polarized LWIR laser. Typical NIR methods such as segmented waveplates could be readily adapted for LWIR wavelengths, although this has yet to be demonstrated. Alternatively, an interferometric technique has been tested at LWIR wavelengths with 70% conversion efficiency [32]. This technique utilizes spiral phase plates to produce $\cos^2\theta$ and $\sin^2\theta$

transverse intensity profiles. Radially polarized light can then be generated by combining a horizontally polarized $\cos^2\theta$ beam with a vertically polarized $\sin^2\theta$ beam, using a waveplate to rotate polarization as necessary. LWIR lasers are particularly well suited for interferometric techniques since the long wavelength causes the necessary phase precision for interferometry to be much easier to achieve.

As discussed earlier, CO_2 is a polarization-insensitive gain medium; thus, this polarization conversion can be performed at low powers before amplification in the CO_2. Due to the polarization sensitivity of gratings, the CO_2 system must be configured in a direct amplification mode instead of a CPA mode. The primary limiting factor of power in this case is nonlinear interaction with the windows that separate the CO_2 tank from the laser transport lines. This can be mitigated by using materials with a low nonlinear index for the windows, such as BaF_2, instead of the typically used NaCl [44].

Looking beyond the proof-of-concept stage, several key advances will need to be made before CO_2 lasers can be a practical daily driver of direct laser accelerators, most notably reaching higher peak powers. Currently, the maximum peak power achieved in a CO_2 laser is 15 TW [33], and the shortest pulse length at terawatt-level peak power is 2 ps [34]. Advances in mid-IR laser technology providing the LWIR seed through optical parameteric amplification for the CO_2 amplifier and adaptation of techniques such as post-compression to LWIR wavelengths [45] have been estimated to allow for a peak power of 0.5 PW, with further improvements possible with coherent beam combining [39]. This is already sufficient power to generate >100 MeV of energy gain, which would enable direct laser acceleration to begin to compete with linacs and wakefield accelerators, with a smaller footprint than the former and potentially higher beam quality than the latter.

5. Conclusions

The ability to generate high-peak-power radially polarized beams is necessary for direct laser acceleration to become viable. However, the problem of injecting external electrons into the accelerating field needs to be solved as well. This has long been an issue for laser wakefield accelerators [46–48] and efficient coupling has only recently been demonstrated [49]. Coupling the electron beam into a direct laser accelerator is even more challenging, particularly for high charge applications, due to the need to couple to the $\sim$2 μm waist of the laser instead of the $\sim$50 μm plasma wavelength of the wakefield accelerator.

The use of LWIR wavelengths, instead of NIR wavelengths, provides a solution for both issues. The gaseous nature of the CO_2 medium provides a pathway to higher power radially polarized beams, and the long wavelength allows the waist size to be an order of magnitude larger. Regardless of the size of the electron beam, the larger waist size of an LWIR laser allows for more efficient transfer of energy to the electron beam, and thus a much higher percentage of usable accelerated electrons.

Even at sub-TW peak powers, which are expected to currently be within reach for CO_2 lasers, MeV-level energy gains can be achieved with a CO_2 laser in the paraxial regime, while preserving typical rf photoinjector beam quality. Thus, radially polarized LWIR lasers provide a pathway to a demonstration of a high-charge, MeV-class vacuum direct laser accelerator. Future work in this vein would consist of constructing a radial polarization converter, demonstrating amplification of the radially polarized light in a CO_2 amplifier, and, finally, showing energy gain when interacting with an electron beam.

Author Contributions: Conceptualization, W.H.L., I.V.P. and M.A.P.; methodology, W.H.L.; software, W.H.L.; validation, W.H.L., I.V.P. and M.A.P.; formal analysis, W.H.L.; investigation, W.H.L.; resources, W.H.L.; data curation, W.H.L.; writing—original draft preparation, W.H.L.; writing—review and editing, W.H.L., I.V.P. and M.A.P.; visualization, W.H.L.; supervision, I.V.P. and M.A.P.; project administration, W.H.L.; funding acquisition, W.H.L., I.V.P. and M.A.P. All authors have read and agreed to the published version of the manuscript.

Funding: This research was funded by the BNL Laboratory Directed Research and Development grant LDRD 24-074 subtask 7 and U.S. Department of Energy Office of Science contract DE-SC0012704.

Institutional Review Board Statement: Not applicable.

Informed Consent Statement: Not applicable.

Data Availability Statement: The raw data supporting the conclusions of this article will be made available by the authors on request.

Conflicts of Interest: The authors declare no conflicts of interest. The funders had no role in the design of the study; in the collection, analyses, or interpretation of data; in the writing of the manuscript; or in the decision to publish the results.

Abbreviations

The following abbreviations are used in this manuscript:

NIR	Near infrared
LWIR	Long-wave infrared
ATF	Accelerator Test Facility
CPA	Chirped pulse amplification

Appendix A. ASTRA Benchmark

We verify the correctness of the radial polarization module built into ASTRA by comparing the maximum energy gain as a function of laser peak power against the simulations performed in ref. [15]. The laser input parameters are $\tau = 7.5$ fs, $w_0 = 2$ µm, and $\lambda = 800$ nm, with an initial electron energy of 10 MeV, corresponding to the parameters used in Figure 6 of ref. [15]. Additionally, we include a simulation carried out with a 9.2 µm CO_2 laser with $\tau = 86$ fs and $w_0 = 23$ µm, which is predicted by the analytic description to have exactly the same energy gain for a given peak power, as τ and w_0 have been scaled up by the ratio of the wavelengths. The carrier-envelope phase and the initial longitudinal separation between the laser and the electron beam were optimized for maximum energy gain, and the simulation was conducted starting 200 Rayleigh ranges before the laser focus and ending 200 Rayleigh ranges after the laser focus.

The results can be seen in Figure A1. The energy gain calculated in ASTRA matches very well with the energy gain calculated in ref. [15], and the Ti:Sa and CO_2 lasers produce identical energy gains. This is in accordance with the predictions of the analytic description of the laser fields.

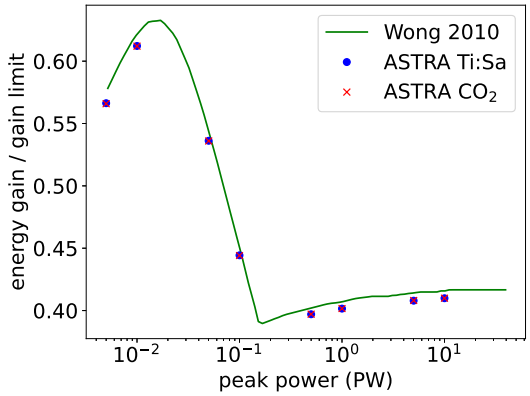

Figure A1. Comparison of the simulations conducted in [15] and a simulated Ti:Sa and CO_2 laser in ASTRA. The laser parameters are listed in the text. We see good agreement between all three sets of simulations, and, notably, the energy gain of the Ti:Sa laser and the CO_2 laser are identical, as predicted.

Appendix B. Comparison of Radially and Linearly Polarized Beams

We compare the performance of a linearly polarized beam and a radially polarized beam for direct laser acceleration in ASTRA simulations. The laser parameters for both cases are $\lambda = 800$ nm, $w_0 = 2$ µm, $\tau = 7.5$ fs, and $P = 10$ TW. We aim to understand

the dynamics at the center of the beam, so we use 2×10^5 macroparticles in a beer can distribution with a length of 1 µm and a diameter of 10 nm, with an initial electron beam energy of 7 MeV. Space charge forces are excluded.

The results are shown in Figure A2. The plot of energy evolution corresponds to the particle with the highest final energy. Both beams show the characteristic deceleration cycle necessary to circumvent the Lawson–Woodward theorem. The linearly polarized beam exhibits more deceleration–acceleration cycles and ends up with lower energy gain and a divergence two orders of magnitude higher. The beam size using the linearly polarized beam grows very quickly, reaching 300 µm in about a millimeter, while the beam size using the radially polarized beam remains below 10 µm. Thus, radial polarization is necessary to preserve beam quality throughout the acceleration process.

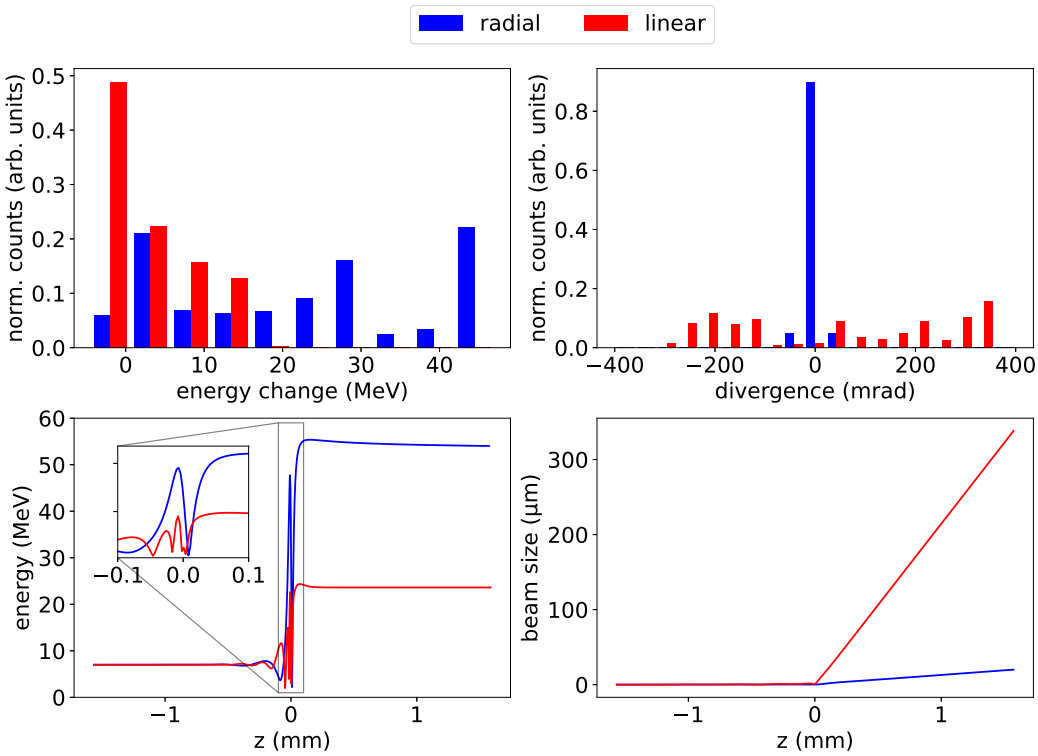

Figure A2. Comparison of a linearly polarized beam and a radially polarized beam. The linearly polarized beam shows noticeably lower energy gain and much higher divergence. The plot of energy evolution corresponds to the particle with the highest final energy. Inset: zoomed-in view of energy oscillations near the focus.

References

1. Peng, F.; Yao, B.; Yan, S.; Zhao, W.; Lei, M. Trapping of Low-Refractive-Index Particles with Azimuthally Polarized Beam. *J. Opt. Soc. Am. B* **2009**, *26*, 2242–2247. [CrossRef]
2. Shvedov, V.; Davoyan, A.R.; Hnatovsky, C.; Engheta, N.; Krolikowski, W. A Long-Range Polarization-Controlled Optical Tractor Beam. *Nat. Photonics* **2014**, *8*, 846–850. [CrossRef]
3. Yang, Y.; Ren, Y.; Chen, M.; Arita, Y.; Rosales-Guzmán, C. Optical Trapping with Structured Light: A Review. *Adv. Photonics* **2021**, *3*, 034001. [CrossRef]
4. Meier, M.; Romano, V.; Feurer, T. Material Processing with Pulsed Radially and Azimuthally Polarized Laser Radiation. *Appl. Phys. A* **2007**, *86*, 329–334. [CrossRef]
5. Niziev, V.G.; Nesterov, A.V. Influence of Beam Polarization on Laser Cutting Efficiency. *J. Phys. D Appl. Phys.* **1999**, *32*, 1455. [CrossRef]
6. Loescher, A.; Oldorf, P.; Peters, R.; Pallmann, W.; Resan, B.; Lesparre, F.; d'Augères, P.B.; Delen, X.; Balembois, F.; Georges, P.; et al. Efficient and High-Throughput Ablation of Platinum Using High-Repetition Rate Radially and Azimuthally Polarized Sub-Picosecond Laser Pulses. *Opt. Express* **2021**, *29*, 19551–19565. [CrossRef]
7. Kraus, M.; Ahmed, M.A.; Michalowski, A.; Voss, A.; Weber, R.; Graf, T. Microdrilling in Steel Using Ultrashort Pulsed Laser Beams with Radial and Azimuthal Polarization. *Opt. Express* **2010**, *18*, 22305–22313. [CrossRef]

8. Dorn, R.; Quabis, S.; Leuchs, G. Sharper Focus for a Radially Polarized Light Beam. *Phys. Rev. Lett.* **2003**, *91*, 233901. [CrossRef]
9. Lerman, G.M.; Levy, U. Effect of Radial Polarization and Apodization on Spot Size under Tight Focusing Conditions. *Opt. Express* **2008**, *16*, 4567–4581. [CrossRef]
10. Varin, C.; Piché, M.; Porras, M.A. Acceleration of Electrons from Rest to GeV Energies by Ultrashort Transverse Magnetic Laser Pulses in Free Space. *Phys. Rev. E* **2005**, *71*, 026603. [CrossRef]
11. Zhan, Q. Cylindrical Vector Beams: From Mathematical Concepts to Applications. *Adv. Opt. Photon.* **2009**, *1*, 1–57. [CrossRef]
12. Carbajo, S.; Nanni, E.A.; Wong, L.J.; Moriena, G.; Keathley, P.D.; Laurent, G.; Miller, R.J.D.; Kärtner, F.X. Direct Longitudinal Laser Acceleration of Electrons in Free Space. *Phys. Rev. Accel. Beams* **2016**, *19*, 021303. [CrossRef]
13. Fortin, P.L.; Piché, M.; Varin, C. Direct-Field Electron Acceleration with Ultrafast Radially Polarized Laser Beams: Scaling Laws and Optimization. *J. Phys. B At. Mol. Opt. Phys.* **2010**, *43*, 025401. [CrossRef]
14. Liu, Y.; Cline, D.; He, P. Vacuum Laser Acceleration Using a Radially Polarized CO_2 Laser Beam. *Nucl. Instruments Methods Phys. Res. Sect. Accel. Spectrom. Detect. Assoc. Equip.* **1999**, *424*, 296–303. [CrossRef]
15. Wong, L.J.; Kärtner, F.X. Direct Acceleration of an Electron in Infinite Vacuum by a Pulsed Radially-Polarized Laser Beam. *Opt. Express* **2010**, *18*, 25035–25051. [CrossRef] [PubMed]
16. Tajima, T.; Yan, X.Q.; Ebisuzaki, T. Wakefield Acceleration. *Rev. Mod. Plasma Phys.* **2020**, *4*, 7. [CrossRef]
17. Tajima, T.; Dawson, J.M. Laser Electron Accelerator. *Phys. Rev. Lett.* **1979**, *43*, 267–270. [[CrossRef]
18. Esarey, E.; Schroeder, C.B.; Leemans, W.P. Physics of Laser-Driven Plasma-Based Electron Accelerators. *Rev. Mod. Phys.* **2009**, *81*, 1229–1285. [CrossRef]
19. Scully, M.O.; Zubairy, M.S. Simple Laser Accelerator: Optics and Particle Dynamics. *Phys. Rev. A* **1991**, *44*, 2656–2663. [CrossRef]
20. Esarey, E.; Sprangle, P.; Krall, J. Laser Acceleration of Electrons in Vacuum. *Phys. Rev. E* **1995**, *52*, 5443–5453. [CrossRef]
21. Steinhauer, L.C.; Kimura, W.D. A New Approach for Laser Particle Acceleration in Vacuum. *J. Appl. Phys.* **1992**, *72*, 3237–3245. [CrossRef]
22. Malka, G.; Lefebvre, E.; Miquel, J.L. Experimental Observation of Electrons Accelerated in Vacuum to Relativistic Energies by a High-Intensity Laser. *Phys. Rev. Lett.* **1997**, *78*, 3314–3317. [CrossRef]
23. Hora, H.; Hoelss, M.; Scheid, W.; Wang, J.W.; Ho, Y.K.; Osman, F.; Castillo, R. Principle of High Accuracy for the Nonlinear Theory of the Acceleration of Electrons in a Vacuum by Lasers at Relativistic Intensities. *Laser Part. Beams* **2000**, *18*, 135–144. [CrossRef]
24. Varin, C.; Payeur, S.; Marceau, V.; Fourmaux, S.; April, A.; Schmidt, B.; Fortin, P.L.; Thiré, N.; Brabec, T.; Légaré, F.; et al. Direct Electron Acceleration with Radially Polarized Laser Beams. *Appl. Sci.* **2013**, *3*, 70–93. [CrossRef]
25. Kong, Q.; Miyazaki, S.; Kawata, S.; Miyauchi, K.; Nakajima, K.; Masuda, S.; Miyanaga, N.; Ho, Y.K. Electron Bunch Acceleration and Trapping by the Ponderomotive Force of an Intense Short-Pulse Laser. *Phys. Plasmas* **2003**, *10*, 4605–4608. [CrossRef]
26. Kong, Q.; Miyazaki, S.; Kawata, S.; Miyauchi, K.; Sakai, K.; Ho, Y.K.; Nakajima, K.; Miyanaga, N.; Limpouch, J.; Andreev, A.A. Electron Bunch Trapping and Compression by an Intense Focused Pulse Laser. *Phys. Rev. E* **2004**, *69*, 056502. [CrossRef]
27. Powell, J.; Jolly, S.W.; Vallières, S.; Fillion-Gourdeau, F.; Payeur, S.; Fourmaux, S.; Lytova, M.; Piché, M.; Ibrahim, H.; MacLean, S.; et al. Relativistic Electrons from Vacuum Laser Acceleration Using Tightly Focused Radially Polarized Beams. *Phys. Rev. Lett.* **2024**, *133*, 155001. [CrossRef]
28. Carbajo, S.; Granados, E.; Schimpf, D.; Sell, A.; Hong, K.H.; Moses, J.; Kärtner, F.X. Efficient Generation of Ultra-Intense Few-Cycle Radially Polarized Laser Pulses. *Opt. Lett.* **2014**, *39*, 2487–2490. [CrossRef]
29. Zhong, H.; Liang, C.; Dai, S.; Huang, J.; Hu, S.; Xu, C.; Qian, L. Polarization-Insensitive, High-Gain Parametric Amplification of Radially Polarized Femtosecond Pulses. *Optica* **2021**, *8*, 62–69. [CrossRef]
30. Zaïm, N.; Guénot, D.; Chopineau, L.; Denoeud, A.; Lundh, O.; Vincenti, H.; Quéré, F.; Faure, J. Interaction of Ultraintense Radially-Polarized Laser Pulses with Plasma Mirrors. *Phys. Rev. X* **2020**, *10*, 041064. [CrossRef]
31. Jana, K.; Mi, Y.; Møller, S.H.; Ko, D.H.; Gholam-Mirzaei, S.; Abdollahpour, D.; Sederberg, S.; Corkum, P.B. Quantum Control of Flying Doughnut Terahertz Pulses. *Sci. Adv.* **2024**, *10*, eadl1803. [CrossRef] [PubMed]
32. Tidwell, S.C.; Kim, G.H.; Kimura, W.D. Efficient Radially Polarized Laser Beam Generation with a Double Interferometer. *Appl. Opt.* **1993**, *32*, 5222–5229. [CrossRef] [PubMed]
33. Haberberger, D.; Tochitsky, S.; Joshi, C. Fifteen Terawatt Picosecond CO_2 Laser System. *Opt. Express* **2010**, *18*, 17865–17875. [CrossRef] [PubMed]
34. Polyanskiy, M.N.; Pogorelsky, I.V.; Babzien, M.; Palmer, M.A. Demonstration of a 2 ps, 5 TW Peak Power, Long-Wave Infrared Laser Based on Chirped-Pulse Amplification with Mixed-Isotope CO_2 Amplifiers. *OSA Contin.* **2020**, *3*, 459–472. [CrossRef]
35. Floettmann, K. A Space Charge Tracking Algorithm. Available online: https://www.desy.de/~mpyflo/ (accessed on 15 October 2024).
36. Marceau, V.; April, A.; Piché, M. Electron Acceleration Driven by Ultrashort and Nonparaxial Radially Polarized Laser Pulses. *Opt. Lett.* **2012**, *37*, 2442–2444. [CrossRef]
37. Palmer, D.T.; Miller, R.H.; Winick, H.; Wang, X.J.; Batchelor, K.; Woodle, M.H.; Ben-Zvi, I. Microwave Measurements and Beam Dynamics Simulations of the BNL/SLAC/UCLA Emittance-Compensated 1.6-Cell Photocathode Rf Gun. In Proceedings of the Electron-Beam Sources and Charged-Particle Optics, SPIE, San Diego, CA, USA, 9–14 July 1995; Volume 2522, pp. 514–526. [CrossRef]

38. Alley, R.; Bharadwaj, V.; Clendenin, J.; Emma, P.; Fisher, A.; Frisch, J.; Kotseroglou, T.; Miller, R.H.; Palmer, D.T.; Schmerge, J.; et al. The Design for the LCLS RF Photoinjector. *Nucl. Instruments Methods Phys. Res. Sect. Accel. Spectrometers Detect. Assoc. Equip.* **1999**, *429*, 324–331. [CrossRef]
39. Polyanskiy, M.N.; Pogorelsky, I.V.; Babzien, M.; Kupfer, R.; Vafaei-Najafabadi, N.; Palmer, M.A. High-Peak-Power Long-Wave Infrared Lasers with CO_2 Amplifiers. *Photonics* **2021**, *8*, 101. [CrossRef]
40. Barber, S. Plasma Wakefield Experiments in the Quasi Nonlinear Regime. Ph.D. Thesis, UCLA, Los Angeles, CA, USA, 2015.
41. Floettmann, K. Some Basic Features of the Beam Emittance. *Phys. Rev. ST Accel. Beams* **2003**, *6*, 034202. [CrossRef]
42. Manahan, G.G.; Habib, A.F.; Scherkl, P.; Delinikolas, P.; Beaton, A.; Knetsch, A.; Karger, O.; Wittig, G.; Heinemann, T.; Sheng, Z.M.; et al. Single-Stage Plasma-Based Correlated Energy Spread Compensation for Ultrahigh 6D Brightness Electron Beams. *Nat. Commun.* **2017**, *8*, 15705. [CrossRef]
43. Di Mitri, S. On the Importance of Electron Beam Brightness in High Gain Free Electron Lasers. *Photonics* **2015**, *2*, 317–341. [CrossRef]
44. Polyanskiy, M.N.; Pogorelsky, I.V.; Babzien, M.; Vodopyanov, K.L.; Palmer, M.A. Nonlinear Refraction and Absorption Properties of Optical Materials for High-Peak-Power Long-Wave-Infrared Lasers. *Opt. Mater. Express* **2024**, *14*, 696–714. [CrossRef]
45. Pogorelsky, I.V.; Polyanskiy, M.N.; Babzien, M.; Simmonds, A.; Palmer, M.A. Terawatt-Class Femtosecond Long-Wave Infrared Laser. *Front. Phys.* **2024**, *12*, 1390225. [CrossRef]
46. van Dijk, W.; Corstens, J.M.; van der Geer, S.B.; van der Wiel, M.J.; Brussaard, G.J.H. Effects of Timing and Stability on Laser Wakefield Acceleration Using External Injection. *Phys. Rev. ST Accel. Beams* **2009**, *12*, 051304. [CrossRef]
47. Urbanus, W.H.; van Dijk, W.; van der Geer, S.B.; Brussaard, G.J.H.; van der Wiel, M.J. Front-to-End Simulations of the Design of a Laser Wakefield Accelerator with External Injection. *J. Appl. Phys.* **2006**, *99*, 114501. [CrossRef]
48. van der Wiel, M.; Luiten, O.; Brussaard, G.; van der Geer, S.; Urbanus, W.; van Dijk, W.; van Oudheusden, T. Laser Wakefield Acceleration: The Injection Issue. Overview and Latest Results. *Philos. Trans. R. Soc. A Math. Phys. Eng. Sci.* **2006**, *364*, 679–687. [CrossRef] [PubMed]
49. Wu, Y.; Hua, J.; Zhou, Z.; Zhang, J.; Liu, S.; Peng, B.; Fang, Y.; Ning, X.; Nie, Z.; Li, F.; et al. High-Throughput Injection–Acceleration of Electron Bunches from a Linear Accelerator to a Laser Wakefield Accelerator. *Nat. Phys.* **2021**, *17*, 801–806. [CrossRef]